3.4 Numerical Investigation of Spark Ignition Processes in Natural Gas Engines with the Advanced Spark Ignition Model

Gunesh Tallu, Michael Frambourg, Matthieu Prouvier, Michael Weißner, Axel Winkler

Abstract

Spark ignition in an internal combustion engine is a complex physical phenomenon, which takes place in a very short time of a few milliseconds but influences the whole succeeding combustion process. A detailed understanding of this process can be gained with the help of experiments focused on ignition or its detailed modelling in Three Dimensional Computational Fluid Dynamics (3D CFD) simulations. A novel modelling approach for spark ignition was presented during 3rd International IAV conference “Ignition Systems for Gasoline Engines” in 2016.

In the extension of the previous study, the present publication focusses on the application of the new model for a monovalent CNG engine with induced ignition. This engine is based on the Volkswagen 4-Cylinder 2.0 litre TDI® Diesel engine converted to operate with homogeneously premixed natural gas air mixture ignited with a serial production spark plug. The engine is operated on the engine test bench at different predefined operating points within the EU funded project GasOn (project # 652816, Horizon2020).

Prior to the spark ignition investigation of this engine, different detailed kinetic mechanisms for natural gas combustion are studied. These mechanisms are analysed for their behaviour in ignition delay and laminar flame speed simulations. From this analysis, suitability of each mechanism for a specific application is derived. Based on this study a mechanism for the current application is chosen. This mechanism is then coupled with the advanced spark ignition model to analyse the spark ignition processes in the CNG engine at different operating points varying only in the relative air-fuel ratio. Good agreement is observed between the simulation results and experimental data.

Kurzfassung

Die Zündung in einem Verbrennungsmotor ist ein komplexes physikalisches Phänomen, welches innerhalb weniger Millisekunden erfolgt aber das gesamte sich

anschließende Verbrennungsverhalten beeinflusst. Ein detailliertes Verständnis dieses Prozesses kann mit Hilfe zündungsspezifischer Experimente und/oder detaillierter Modellierung innerhalb dreidimensionaler Strömungssimulationen gewonnen werden. Ein neuentwickelter Modellierungsansatz für den Zündprozess wurde während der 3 Internationalen IAV-Tagung “Zündsysteme für Ottomotoren” in 2016 erstmalig vorgestellt.

Als Erweiterung zu der vorherigen Studie wird in der vorliegenden Veröffentlichung als Anwendungsfall für das neue Zündmodell ein monovalenter CNG-Motor mit Fremdzündung behandelt. Der Motor basiert auf dem 4-Zylinder Volkswagen 2.0 Liter TDI® Dieselmotor, der nach einer Umrüstung mit einer homogenen Erdgas-Luft Mischung betrieben und das Gemisch mit einer Serien-Zündkerze gezündet wird. Im Rahmen des EU-Projektes GasOn (Projekt-Nr.: 652816, Horizon2020) wird der Motor am Motorprüfstand bei unterschiedlichen vordefinierten Betriebspunkten gefahren.

Im Vorfeld der Analyse der Zündung des Motors werden unterschiedliche detaillierte Reaktionsmechanismen für Erdgas betrachtet. Die Mechanismen werden hinsichtlich Zündverzug und laminarer Flammengeschwindigkeit evaluiert. Auf dieser Basis wird ein Mechanismus für die aktuelle Applikation ausgewählt. Dieser Mechanismus wird mit dem neuartigen Zündmodell gekoppelt, um den Zündprozess im Versuchsträger bei unterschiedlichen Betriebspunkten zu untersuchen. Für eine Lambda-Variation wird eine gute Übereinstimmung zwischen Messung und Simulation erreicht.

1 Introduction

1.1 Motivation for Monovalent CNG Engines

Increasing demand for lowering CO_2 emissions has led to the need of improved technologies for the automotive sector. Besides the new electric mobility solutions, which will become more present on the market in the future, the internal combustion engines will remain the most important part of the powertrain for next decades. Compressed Natural Gas (CNG) has two main advantages of high knock resistance and low CO_2 emissions. High knock resistance is not being exploited in the state of the art bivalent CNG engines to the fullest. Designing an engine, mainly for CNG, with higher compression ratio and an improved ignition system will lead to a significant CO_2 reduction of up to 25% compared to a diesel engine. Especially for lean conditions, besides other factors, the ignition is a key challenge to realize a stable and complete combustion. Therefore, there is a need to investigate the ignition process in detail.

1.2 Need of Ignition Modelling

For spark ignited (SI) engines, the capability of emission reduction lies on a number of factors. One of them is the successful ignition of the charge in a wide range of operating conditions. The spark ignition is a complex physical phenomenon which takes place in a very short time (milliseconds), but influences the whole succeeding combustion process. A detailed understanding of this process can be gained with

the help of ignition focused experiments or detailed modelling in Three Dimensional Computational Fluid Dynamics (3D CFD) simulations.

In state of the art 3D CFD combustion simulations, ignition is achieved through the introduction of a substantial amount of energy at the predefined spark plug position at a given point in time (spark ignition timing). It is considered that the ignition is always successful and, after reaching a predefined size, the flame kernel is converted into a fully propagating flame. This approach is simple but not sufficient to correctly reproduce physical effects of the flow field and mixture conditions in the near spark plug area on the inflammation phenomena and subsequent flame propagation process. Hence, detailed 3D CFD modelling based on the physics of the ignition phenomena taking place over the spark duration is required.

Details on the development of the novel modelling approach for spark ignition can be found in [1]. This model is summed up here in Section 2. In the extension of the previous study, the presented model is here applied for the analysis of a spark plug ignited natural gas engine.

2 Advanced Spark Ignition Model

An overview of the spark ignition phenomenon is described in short. The spark ignition phenomenon takes place in three phases: breakdown, arc discharge and glow discharge. These are utilised to characterise any type of coil ignition system. Changes in voltage and current over the spark duration signify these three phases. In the breakdown phase, lasting nanoseconds, large rise in the voltage in very short time is seen. Here, the initial electrical contact between the electrodes takes place. In the arc discharge phase, drop in the current and voltage is observed due to the arcing between the electrodes. Finally, in the glow discharge phase, visual glow is seen with a drop in current, whereas a rise in the voltage is observed. In these three phases, inflammation takes place at different stages. This starts from the plasma formation and its expansion in the breakdown phase. Subsequently, with the exchange of initial radicals of C, H, O and N between the cooling plasma and the surrounding, initial combustion reactions are started. Chemical energy support from these reactions increases gradually, which is termed as flame kernel, and finally it should be sufficient enough to cater to the turbulence in the surrounding. After the spark discharge duration, the flame kernel then converts into a fully propagating turbulent flame. [2]

The advanced spark ignition model numerically describes the above stated spark ignition phenomenon in 3D CFD simulations. The model can be sub-divided into three different parts. They are flame kernel initialisation, flame kernel growth and transfer to turbulent combustion model. In the first sub-model, effects of discharge of breakdown energy, plasma formation and expansion are modelled. Depending upon the breakdown energy from the ignition coil, the relative air-fuel ratio (λ) in the surrounding and the plasma temperature, the initial flame kernel size at the time of spark ignition is determined. This flame kernel is represented with Lagrangian marker particles between the spark plug electrodes. Throughout the application of the model, this approach is utilised to capture the interaction between the flow field in the surrounding and the flame kernel.

In the next part of the model, increased contribution of the flame kernel in the form of chemical energy is considered and the change in the size of the flame kernel over the arc discharge and glow discharge duration is computed. For this purpose, the spark discharge power, the changes in the flame kernel specific heat, the changes in the pressure and the specific heat of the surrounding are accounted for the calculation of the chemical source term in the mass and the energy conservation equations. Closure of these equations is achieved with the help of the flame kernel speed model. This model comprises of laminar flame speed, velocity contribution of the plasma and a correlation between laminar and turbulent flame speed as per Herweg et al. in [3].

Before the initial size of the fully propagating flame is given as an output from the advanced spark ignition model to the level-set G-equation turbulent combustion model, few conditions are checked. The critical flame kernel radius, which caters mainly as the least progress parameter for the flame kernel, is calculated throughout the spark discharge duration. This parameter directly correlates growth of the flame kernel with mixture conditions and turbulence in the surrounding flow field. Another parameter is the flame kernel movement, which considers only the effect of turbulence in the flow field on the flame kernel disposition. Over the spark discharge duration, if the flame kernel movement exceeds a predefined experimental value then the spark ignition model can predict an event of restrike. After successful completion of these two conditions, transfer from the spark ignition model to the turbulent combustion model takes place.

To consider the effects of detailed chemical kinetics on the flame kernel growth, the specific heat capacity of the flame kernel and the laminar flame speed are calculated in advance in form of tables with different detailed chemical kinetic mechanisms at different mixture conditions (varying in λ, pressure, temperature and exhaust gas recirculation ratio (ψ)). These mixture conditions are studied before hand from the 3D CFD engine simulations. Then the pre-calculated tables are coupled with the spark ignition model to read the values of these properties for each cell in the flame kernel as per its conditions. Study and selection of the detailed chemical kinetic mechanism for this engine case is discussed in the next section.

3 Study of Detailed Mechanisms

Study of different detailed mechanisms for their individual behaviour in terms of ignition delay and laminar flame speed are presented in this section. For this purpose, suitable experiments of ignition delay and laminar flame speed are simulated with 0D and 1D chemistry solvers. Rather than selecting a mechanism suitable for the application, mechanisms are at first analysed for their individual advantages and drawbacks.

The CNG utilised for the investigations at the engine test bench is a typical H-Gas, which includes methane up to 90%. Therefore, in all the simulations, CNG is represented by the properties of methane. Three different detailed kinetic mechanisms for methane or natural gas combustion are considered for this study. Table 1 lists these mechanisms with their individual application range of pressure, temperature and equivalence ratio (ϕ). First of them, MFC, is the mechanism developed by Reaction Design (Ansys Inc.) within the Model Fuel Consortium. This

mechanism is mainly developed for combustion of C_1-C_5 hydrocarbons and is validated extensively for its application range. The application range is wider compared to current application, with the widest temperature applicability amongst the three mechanisms. GRI, is a well known mechanism for natural gas combustion, developed by Gas Research Institute of University of California, Berkley. The widest application range amongst the three mechanisms over ϕ is observed for this mechanism. Lastly, a mechanism from chemistry solution experts from Sweden, LOGE AB developed for combustion of C_1-C_5 hydrocarbons is considered in this study. This mechanism can be applied over the widest pressure range.[4], [5], [6]

Table 1: Application range of detailed chemical kinetic mechanisms [4], [5], [6]

Mechanism	Species	Reactions	Application Range		
			Temperature [K]	ϕ [-]	Pressure [bar]
MFC [4]	528	3214	298 - 1800	0.3 - 4.0	0.6 - 60.0
GRI [5]	53	350	1000 - 2500	0.1 - 5.0	0.1 - 20.0
LOGE [6]	362	3449	600 - 1400	0.1 - 3.0	1.0 - 120.0

3.1 Ignition Delay Time

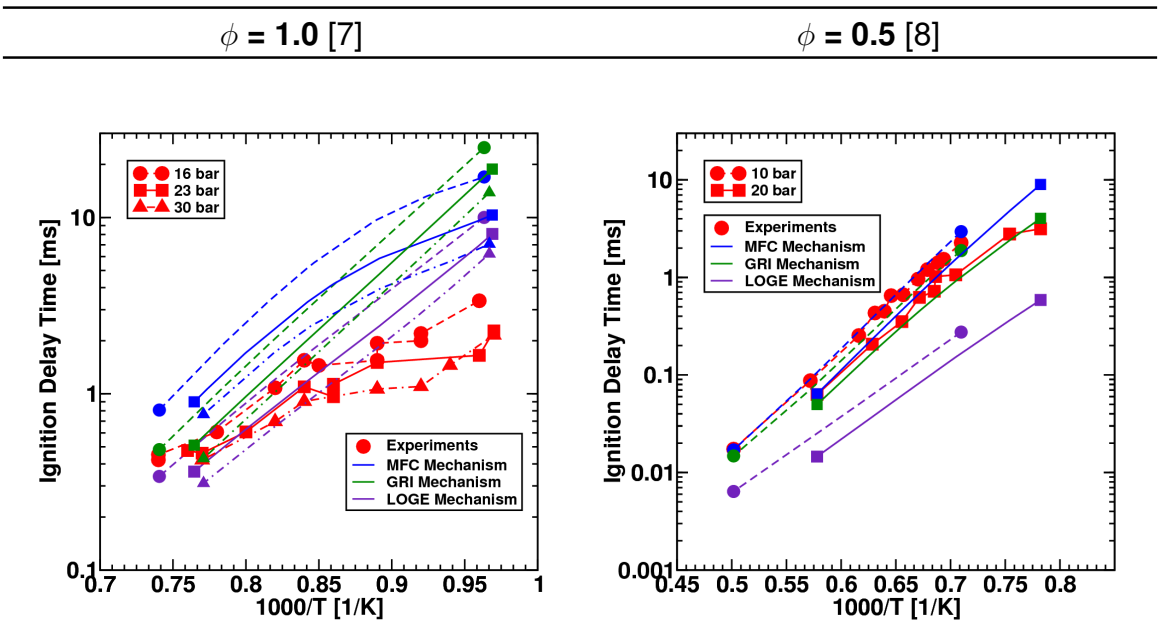


Figure 1: Comparison of detailed chemical kinetic mechanisms for ignition delay time against experiments in [7] (left) and [8] (right)

First of all, a comparison of the simulation results for ignition delay time with the three mechanisms is presented in Figure 1 in the form of ignition delay diagram. Here, as per the current application, two different experiments for methane by Huang et al. [7]

(Figure 1, left) at stoichiometric conditions and Zhang et al. [8] (Figure 1, right) at ϕ = 0.5 are simulated. For both set of results, it can be seen that, as the pressure increases, ignition delay time decreases. With the change in temperature from 1000 K to 2000 K, ignition delay decreases. These fundamental behaviours are reproduced by all the three mechanisms. Further, for the stoichiometric conditions, a typical negative temperature behaviour in the temperature range between 1000 K and 1200 K is observed. With the comparison of simulation results, at three pressure levels, only the MFC mechanism could reproduce this behaviour but with substantial difference against the experimental data. This behaviour at relatively higher temperature needs further experimental investigation. Overall in the higher temperature region, experimental results are reproduced by the simulation with MFC and GRI mechanisms, whereas at relatively lower temperature, simulation results with LOGE mechanism are closer to the experimental data. The results for lean conditions show that, for both pressure levels at higher temperature, simulation results with MFC and GRI mechanisms are in good accordance with the experimental data. For intermediate temperature range, difference between simulation and experiments is least for GRI mechanism.

3.2 Laminar Flame Speed

A comparison between simulation results and experimental data for laminar flame speed is presented in Figure 2. Here, the behaviour of the laminar fame speed against variation in pressure (Figure 2, Left) and variation in ϕ (Figure 2, Right) from Elia et al. in [9] is studied. With increase in pressure, decrease in the laminar flame speed is observed and change in the equivalence ratio away from stoichiometric condition results in decrease in the laminar flame speed. These behaviours are reproduced by all the three mechanisms. Analysing the results for the variation in pressure, it is observed that, over the whole range of pressure variation, simulation results with LOGE and GRI mechanisms are in good accordance with the experimental results. With variation in ϕ, it can be seen that, at and near stoichiometric conditions, the experimental data is reproduced with good accuracy by the simulation results of GRI and MFC mechanisms. However, as the conditions diverge from this equivalence ratio area, simulation results with LOGE mechanism are able to reproduce the experimental data accurately.

Summarizing these results, it can be seen that, each mechanism has its own forte in different areas. MFC mechanism is found suitable for reproduction of ignition delay results at higher temperature range and lean mixtures as well as the NTC behaviour, whereas it can also reproduce the laminar flame speed near stoichiometric mixture composition and at lower pressures. GRI mechanism is suitable at the higher pressure conditions for both ignition delay time and laminar flame speed. LOGE mechanism is rather applicable in intermediate temperature and pressure range for ignition delay time simulations and can be used in rich and lean mixture conditions for laminar flame speed simulations. Therefore, based on these findings, three mechanisms are further evaluated for the suitability of their results in direct coupling with the advanced spark ignition model in 3D CFD simulations and these results are presented in section 4.4.

Temp. = 470 K, ϕ = 1.0 [9]	**Pressure = 1 bar, Temp. = 298 K** [9]

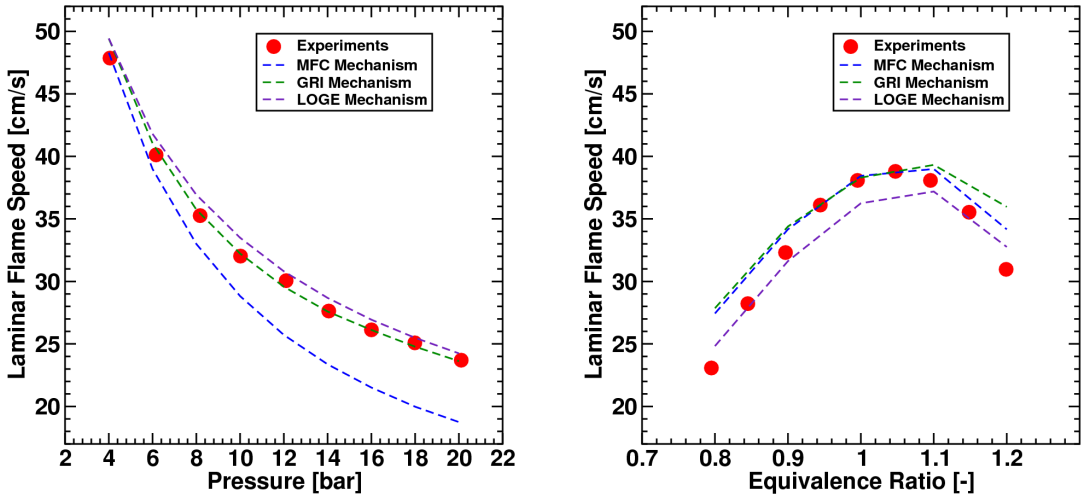


Figure 2: Comparison of detailed chemical kinetic mechanisms for laminar flame speed against experiments in [9] for pressure variation (left) and variation in equivalence ratio (right)

4 Model Application on Engine Case

4.1 Engine Details

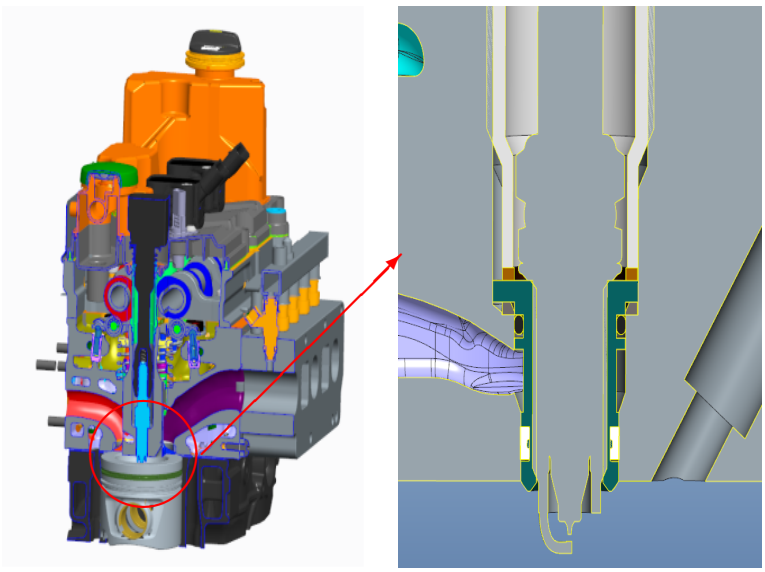


Figure 3: Depiction of the engine with central position of spark plug

As stated in Section 1, a monovalent CNG engine can exploit the property of the high knock resistance of CNG to the fullest. This can be done by an early centre of combustion and/ or with a higher compression ratio. The engine used in this project is

based on the Volkswagen 2.0 litre diesel engine as explained by Neusser et al. in [10], which is very robust and capable of peak cylinder pressures of up to 190bar. Engine bore and stroke are 81.0mm x 95.5mm. The compression ratio has been modified to 14.5 by a new piston bowl. As shown in Figure 3, the spark plug is located centrally in the place of the former diesel injector and supplied with electric energy by a standard ignition coil. The engine is run on premixed homogeneous mixture of air and CNG. For this purpose, a gas mixer from Heinzmann as given in [11] is utilised. The engine manifolds are further modified to adapt to this new type of combustion process. For the purpose of measurement on the engine test bench, pressure sensors from Kistler of Type 6041A are utilised on all the 4 cylinders, whereas the intake manifold of cylinder 1 is equipped with an uncooled pressure sensor from Kistler of type 4007C. The exhaust pressure of cylinder 1 is measured with a cooled pressure sensor from Kistler of type 4011A. A Lambda sensor is mounted behind the turbine. For each operating point, at least 300 fired cycles are utilised for further investigation.

4.2 Details of Operating Points

As stated in Section 1, one of the advantages of such a combustion system is the leaning of the mixture, leading to a reduction in fuel consumption and an increase in the efficiency of the engine. Nevertheless, it is to investigate if there is a limit in leaning the mixture at which the engine still runs stable.

For this purpose, three engine operating points labelled as A, B, and C are defined, in such a way that they represent a variation only in the premixed natural gas air mixture. Description of the relevant parameters for the operating points is listed in Table 2. The centre of combustion is kept constant at 8° CA after Top Dead Centre (aTDC) and hence, accordingly with the increase in the value of λ, Spark ignition Timing (ST) is advanced.

Table 2: Details of operating points selected for simulation

Parameter	Value		
Operating Point	A	B	C
Speed [rpm]	1500		
Load [Nm]	100		
λ [-]	1.0	1.5	1.8
Intake manifold pressure [bar]	0.74	0.95	1.20
Spark ignition timing [° CA bTDC]	17.2	27.2	52.8

4.3 3D CFD Simulation Setup

The setup for 3D CFD simulation of the above-stated operating points of the engine with the help of the software VECTIS from Ricardo Software is described here. For this purpose, representative geometry of a single cylinder with intake and exhaust port

is considered in the simulation domain. Figure 4 shows the discretization of the geometry at TDC. Here it is seen that, the exhaust port (right) and the intake port (left) are discretized with a Cartesian mesh with a cell size of 2 mm, whereas a mesh cell size in the cylinder geometry (centre) of 1 mm is chosen. For the purpose of complete geometrical representation of the spark plug electrodes, the cell size near the spark plug is kept to 0.5 mm. The properties of methane are used for the representation of natural gas in the simulation domain. As discussed above, natural gas and air mixing takes place in the gas mixer at least 0.5 m before the inlet of intake manifold. Therefore, it is assumed that air and natural gas are homogeneously mixed when they enter the intake port. Accordingly, the mass flow rate at each degree crank angle of homogeneous air natural gas mixture at individual λ is utilised as inlet boundary condition on the intake port inlet. This mass flow rate is generated from 1D CFD simulation. On the exhaust port outlet side, averaged measured pressure on engine exhaust port at every 0.5° CA for one four stroke cycle is utilised. Starting from the maximum exhaust valve opening at 245° CA aTDC (245° CA) till 80° CA aTDC (800° CA), the simulation is carried out with moving mesh for piston, intake and exhaust valves. The timestep utilised over the whole simulation is 0.01° CA and it is reduced to 0.005° CA during the phases of ignition and combustion.

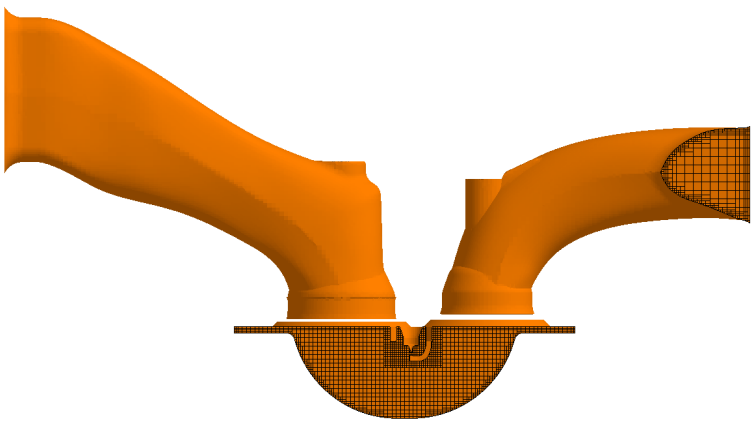


Figure 4: Simulation domain with single cylinder at TDC (centre) including intake port (left) and exhaust port (right)

4.4 Comparison of Mechanisms in 3D CFD Engine Simulation

In addition to the comparison presented in Section 3, the mechanisms are compared in the conjunction to their application with the advanced spark ignition model in the 3D CFD simulation. Aim of this study is also to analyse the effect of different detailed mechanisms on the spark ignition process on the basis of Operating Point (OP) A. For this purpose, as stated in Section 2, Combustion Progress Variable (CPV) and laminar flame speed tables for the three selected mechanisms over the application parameter range are generated. The details of these pre-calculated tables can be found in Table 3. Numbers in the brackets show the interval at which each parameter is incremented over the range of that parameter in the tabulation. The range of each parameter is selected based on the engine simulations till the spark ignition timing, which are presented for OP A hereafter.

Table 3: Range of parameters for pre-calculated CPV and laminar flame speed tables for study of kinetic mechanisms in the engine

Table	Pressure [bar]	Temperature [K]	ϕ [-]	ψ [%]
CPV	1 - 90 (15)	500 - 1500 (100)	0.5 - 1.2 (0.1)	0 - 10 (10)
Laminar Flame Speed	1 - 40 (10)	300 - 800 (100)	0.5 - 1.3 (0.2)	0 - 10 (10)

Before comparing the results obtained with the detailed mechanisms, it is important to analyse the conditions in the combustion chamber till spark ignition timing. Figure 5 shows the mixture conditions and flow field at the spark ignition timing for OP A. A homogeneous distribution of the fuel mass representing the stoichiometric mixture in the combustion chamber is observed. This suggests that the homogeneity of the mixture is held intact till the spark ignition timing. The distribution of Turbuelnt kinetic energy (TKE) is plotted in the top right sub-figure. It is observed that overall turbulence level is low in the combustion chamber. Intermediate turbulence level is observed in the top central part of the combustion chamber besides the spark plug. With the help of velocities plotted on the central plane of the combustion chamber and in the spark plug electrode gap, it can be observed that a typical diesel swirl motion is not present in this case. Rather a flow field colliding at the centre of the combustion chamber from both sides is present.

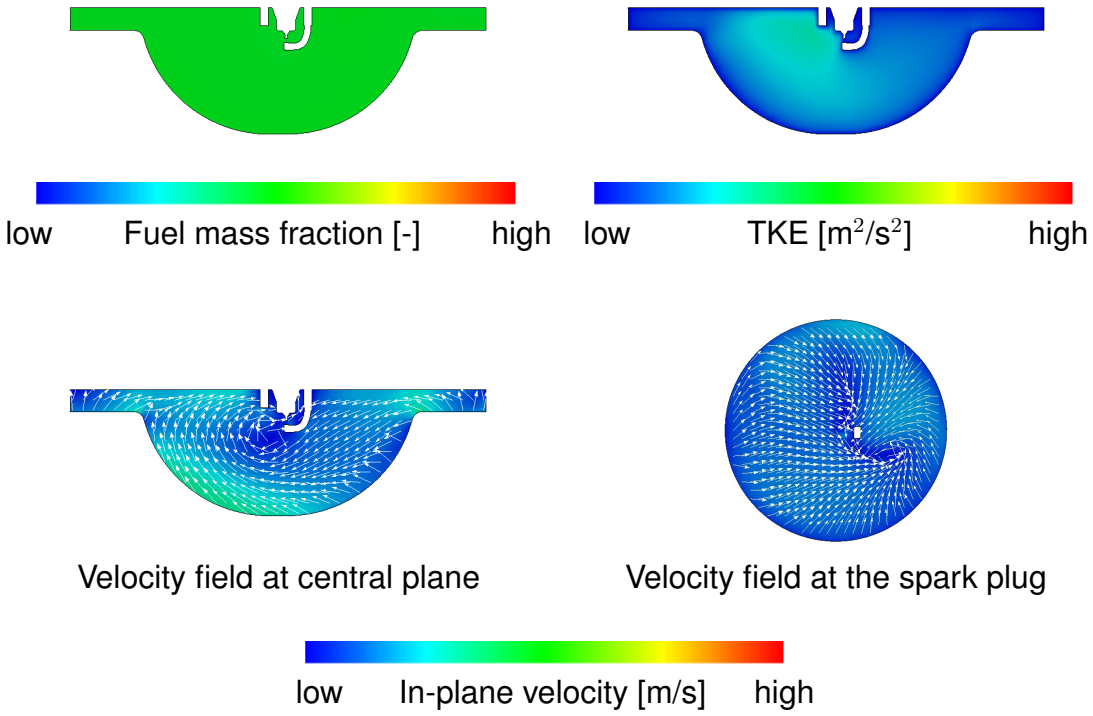


Figure 5: Conditions in the combustion chamber at spark ignition timing for OP A (703° CA)

On the basis of this analysis, a study of the selected detailed chemical mechanisms is carried out. For this purpose, results of the advanced spark ignition model in the form

of the flame kernel radius are compared. Figure 6 presents this comparison for simulations without detailed mechanism (1-step mechanism) and with the three selected mechanisms after Spark ignition Timing (aST) till the end of spark discharge duration of 2 ms which are 18° CA for engine speed of 1500 rpm. For individual simulations, results of the flame kernel radius are plotted only till its transition into the flame. Faster growth of the flame kernel is predicted by both MFC and LOGE mechanisms than that of GRI and 1-Step mechanisms. Therefore, for these two cases, the flame kernel reaches the size required for its transition into the flame at least 5° CA earlier than that of for GRI and one step mechanisms. These results can be correlated back to the simulation results of the ignition delay and the laminar flame speed for detailed mechanisms from section 3. It can be seen that, these two mechanisms (LOGE and MFC) either over-predict the laminar flame speed or under-predict the ignition delay time for respective conditions in the engine experiments.

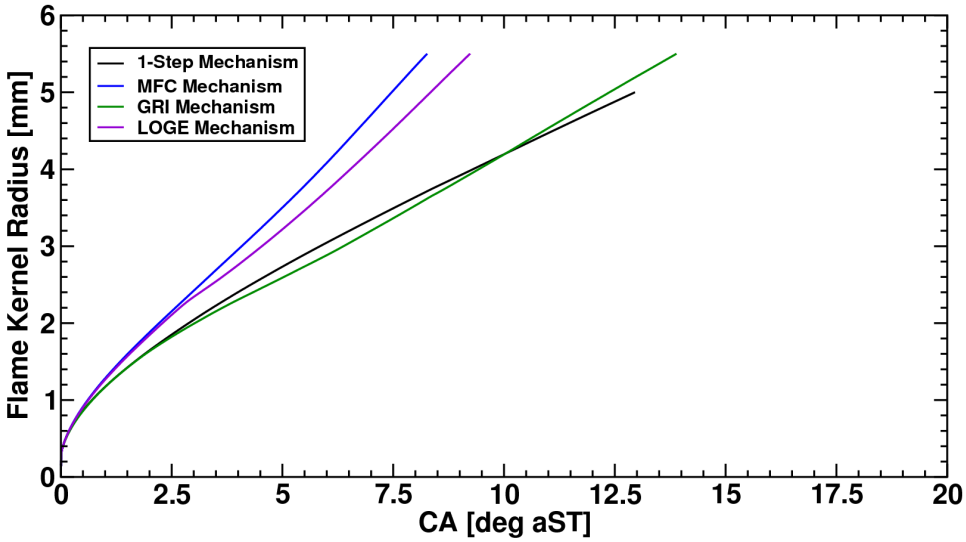


Figure 6: Flame kernel radius over time for OP A for simulations without detailed mechanism and with the three detailed mechanisms

Figure 7 shows the comparison of the simulated pressure curves without detailed chemical kinetic mechanism and with the three studied mechanisms against the experimental data. It can be seen that, all the simulation results (with and without detailed mechanisms) are in very good agreement with the experimental data in the initial phase of the combustion after the spark ignition timing. Later, the simulation results deviate for individual cases of detailed mechanisms. The simulation results with GRI mechanism are in good accordance with the experimental data. The simulation results with the 1-step mechanism (without detailed mechanism) can also reproduce the experimental data with good accuracy. Rather the simulation results with MFC and LOGE mechanism overpredict the maximum cylinder pressure as well as the pressure decrease in the expansion phase. Similar to the results of the flame kernel radius, these results can be deduced again with the results from section 3. Therefore, from this comparison GRI mechanism is utilised for the further analysis.

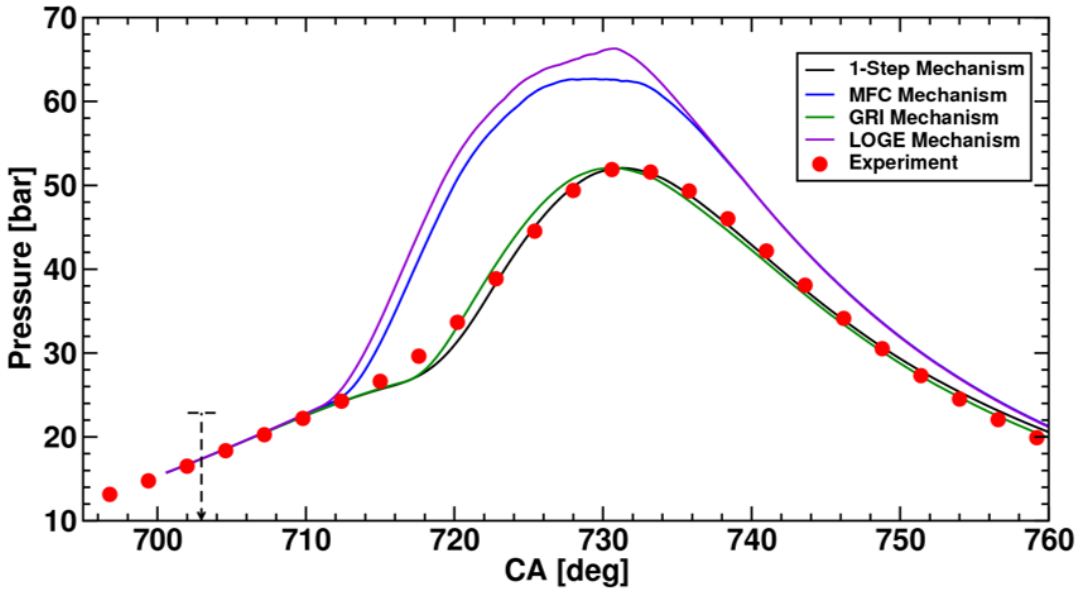


Figure 7: Comparison between simulation results without detailed chemical kinetics, with three detailed kinetic mechanisms and experimental data for cylinder pressure of OP A; Arrow indicates the spark ignition timing for OP A

4.5 Results of 3D CFD Engine Simulation

Results of the 3D CFD engine simulation with the selected detailed kinetic mechanism are presented in this section. To study the behaviour of the advanced spark ignition model for different values of λ over the stable engine operating range, results for operating points A, B and C are compared.

Similar to the previous study, conditions in the combustion chamber at spark ignition timing are analysed for OP B and OP C in Figure 8. With the help of an adjusted scaling of green area representing stoichiometric air fuel mixture, homogeneous fuel distribution of respective values of λ is observed for both operating points. Distribution of TKE and the velocity fields are similar to OP A for both operating points. The differences observed are mainly due to the difference in the spark ignition timing and hence resulting into the different timing of analysis in the compression stroke. Quantitative comparison of different parameters in the vicinity of the spark plug also showed very less changes except the differences pertaining to the changes due to different values of λ. Another effect of the different spark ignition timings and the different intake manifold pressure (as given in Table 2) is the difference in the cylinder pressure at spark ignition timing. This can be seen in Figure 11. At the time of spark ignition for each operating point, depicted with the arrow of individual colour, as the value of λ increases, due to increase in the intake manifold pressure, increase in the cylinder pressure at the individual spark ignition timing is observed. Detailed discussion of results presented in Figure 11 is carried out separately later in this section.

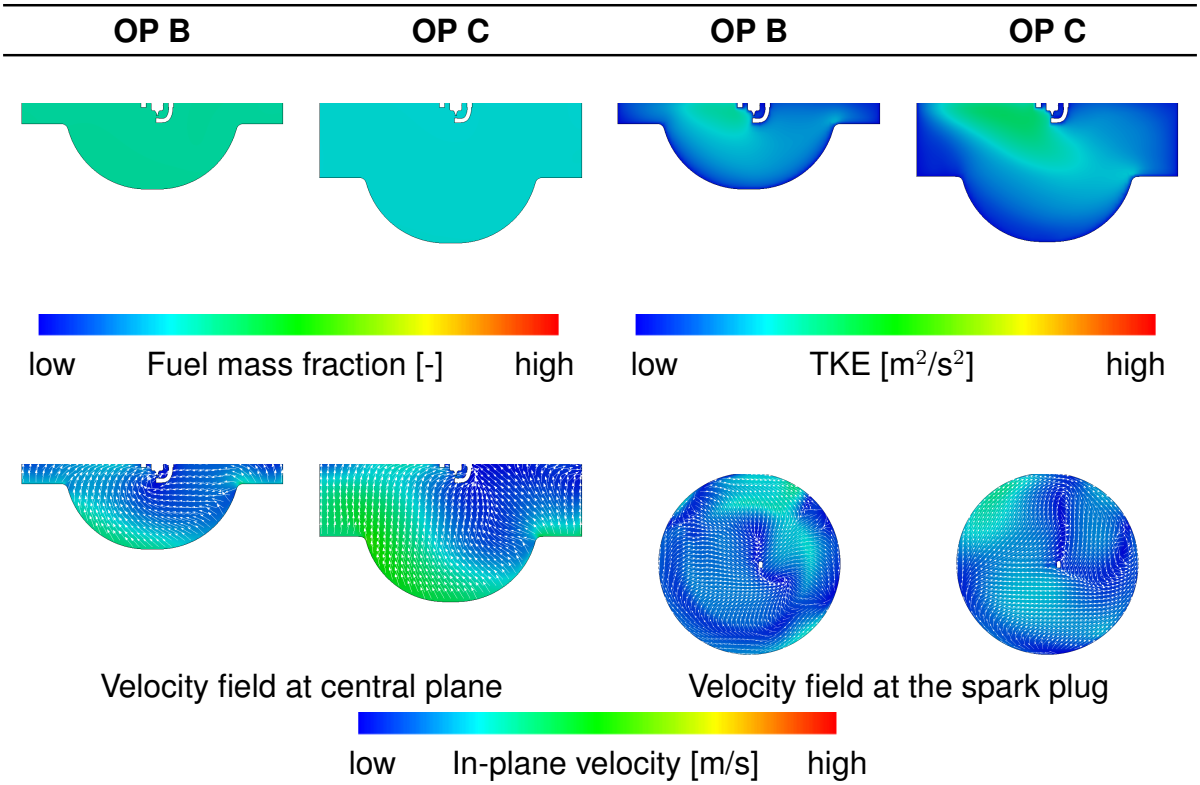


Figure 8: Conditions at spark ignition timing for OP B (692.5° CA left) and OP C (668° CA right)

Initial results of the advanced spark ignition model in the form of the flame kernel development over the spark discharge duration for three operating points are shown in Figure 9. Here, the growth of the flame kernel is plotted only till its transition into a fully propagating flame. It is seen that, as the value of λ increases, the final flame kernel radius before its transition into the flame decreases. This can be correlated with the results of laminar flame speed in Section 3.2, where, deviation from stoichiometric mixture conditions results in a decrease in the laminar flame speed. Analysing these results in detail, it can be seen that, for OP A (λ = 1.0), the required size of the flame kernel for its transition into fully propagating flame is achieved earlier ($\sim$14° CA aST) than other operating points. This transition time is based on the parameters such as, mixture strength, flow field conditions and pressure in the surrounding. As the difference between the transition time for OP A and that for other operating points is large, the dominating factor for the transition time is the mixture condition. Least difference in the transition time for OP B and OP C is observed, as in this comparison, changes in pressure at the spark timing are more effective than that of changes in the mixture condition. This shows that the advanced spark ignition model gives one parameter i.e. flame kernel radius, which relates all the conditions in the surrounding against the progress of the spark ignition process in the engine.

Results of the flame kernel progress are visualised in Figure 10 with the help of representation of the G-Scalar over the spark duration for the three operating points OP A, OP B and OP C. Here, it should be noted that, in case of the advanced spark ignition model, for the purpose of representation, the envelope of scalar G with the value equal to zero is created around the current flame kernel position. This should

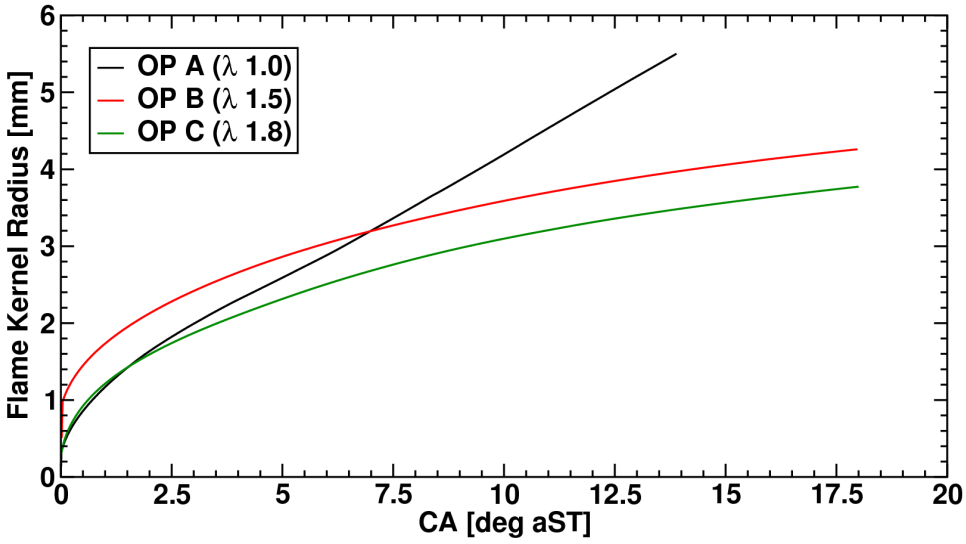
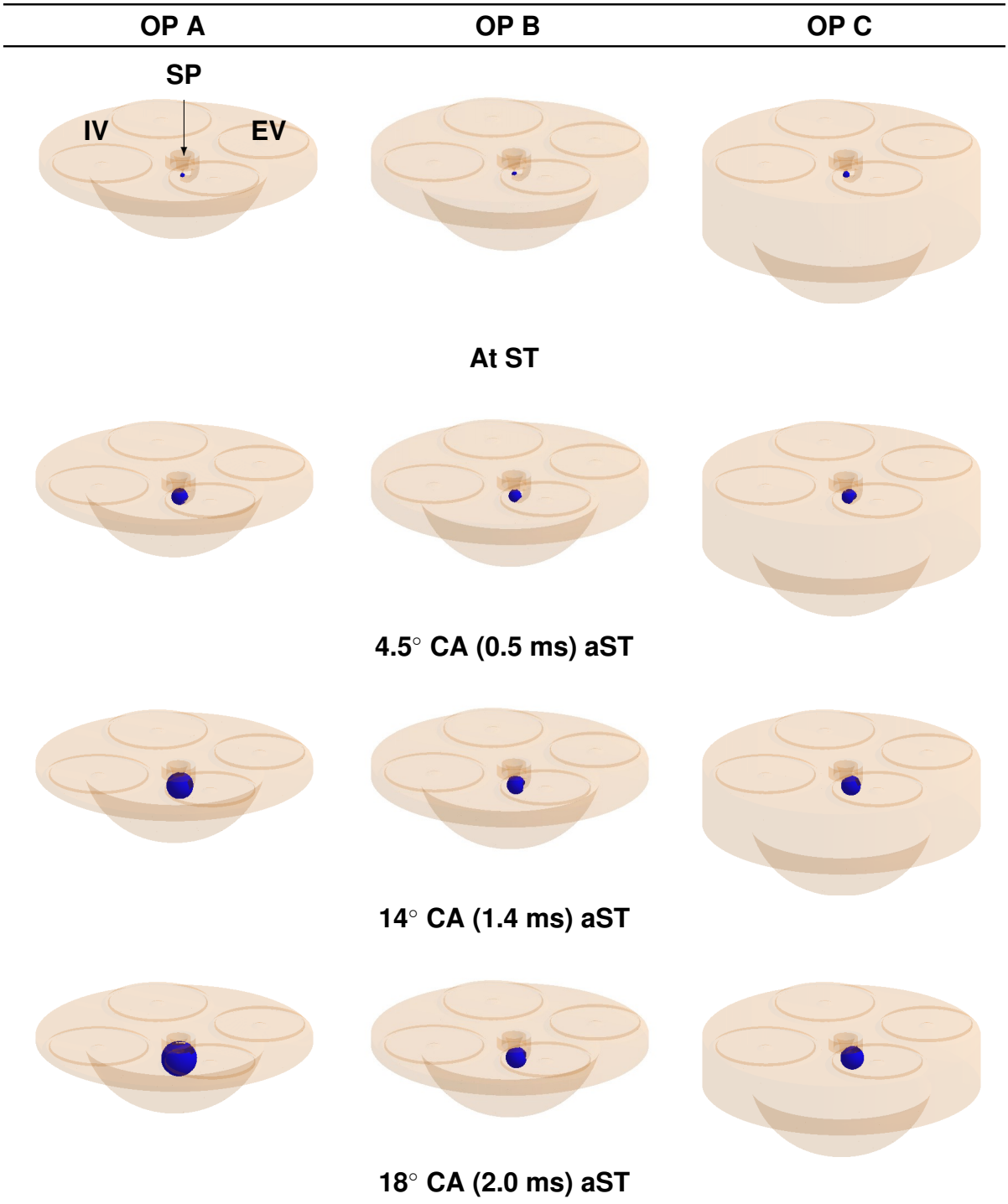


Figure 9: Flame kernel radius over time for OP A (λ 1.0), OP B (λ 1.5) and OP C (λ 1.8)

not be confused with the approach, where G scalar directly represents the flame surface. For the purpose of frame of reference, locations of the spark plug (in the centre), the intake valves (on the left side of the spark plug) and the exhaust valves (on the right side of the spark plug) are shown in one of the representations. At individual spark timing, comparatively smaller but still differential sizes of flame kernel are found for each operating point. At 4.5° CA aST, for stoichiometric conditions, comparatively larger growth of the flame kernel in this duration is observed. This trend continues till 13° CA aST, which results in the transition of the flame kernel in the fully propagating flame. At this point of time, for other operating points, the flame kernel size is still attaining this minimal flame kernel size for the transition. At the end of the discharge duration, at 18° CA (2.0 ms) aST, OP B and OP C have attained this size, and are on the verge of transition. Here at this point of time, but for OP A, the growth in the already transited flame size is observed. These results can be correlated with the results discussed above and hence, validate each other.

Results in the form of comparison of cylinder pressure between experimental data and simulation results for the considered three operating points are presented in Figure 11. It can be seen that, at the spark ignition timing for all the operating points experimental data and simulation results are in very good agreement. This indicates that the simulation method and the boundary conditions utilised for this engine simulation are appropriate. Furthermore, overall combustion simulation results are in good accordance with experimental data. As discussed before, due to the increased air requirement for the leaning of the mixture, intake manifold pressure is increased for a higher value of λ. Effectively this results in the higher maximum combustion pressure. This trend, as observed in the experimental data, is reproduced by the simulation results. Spark ignition and initial phases of the combustion are reproduced accurately for all the three operating points by this simulation method. Apart from the results of OP C, the maximum pressure and its timing are predicted accurately by the simulation. In the case of OP C, value of maximum pressure is correctly reproduced but an early pressure rise resulting in an offset in the timing of maximum pressure by



Iso-Surface G=0 representing flame kernel or flame for sub-figure of OP A at 18° CA aST

Figure 10: Flame kernel growth for OP A (λ 1.0), OP B (λ 1.5) and OP C (λ 1.8); IV: Intake Valve, EV: Exhaust Valve, SP: Spark Plug, ST: Spark Ignition Timing

4.8° CA is observed. This can be correlated with the fact that, as shown in Figure 2 (right), at lean conditions, the difference between the simulated and the experimental laminar flame speed is increasing. Similar differences are also seen in the expansion phase, where for OP A the simulation results show a faster drop of pressure compared to the experimental data.

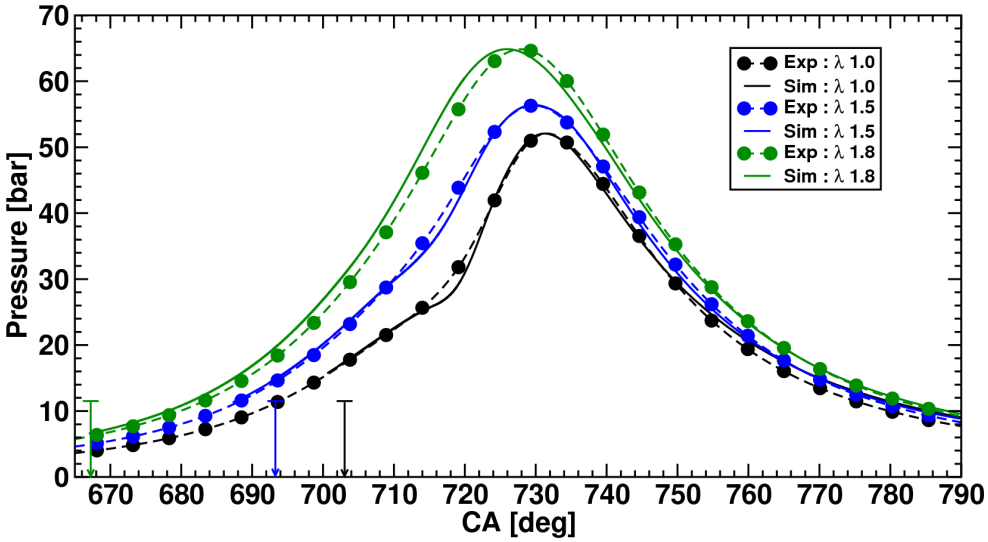


Figure 11: Comparison of cylinder pressure between simulation results and experimental data for OP A (λ 1.0), OP B (λ 1.5) and OP C (λ 1.8) with arrows showing the spark ignition timing for each OP

5 Conclusion

In this paper, the previously presented approach of modelling of the spark ignition is further validated on a natural gas engine. The Volkswagen 2.0 litre serial diesel engine is modified to be operated as a monovalent natural gas engine ignited with a serial spark plug. Engine operating points are chosen in such a way that they represent only a variation in the relative air-fuel ratio at same load and speed. These points are calculated with the help of the advanced spark ignition model in the 3D CFD simulations.

For the purpose of simulation with the advanced ignition model, priorly, a comparative study of 3 available natural gas combustion mechanisms for ignition delay time and laminar flame speed for different experimental conditions is carried out. MFC mechanism is found suitable for the engine operational temperature range, whereas GRI mechanism is seen appropriate at high pressure conditions. LOGE mechanism shows its suitability over the broader equivalence ratio. These three mechanisms are further analysed in the 3D CFD simulation of one engine operating point, OP A. With the help of tabulation approach, these detailed mechanisms are coupled in 3D CFD simulations. Here, comparison of the simulation results against experimental data shows that GRI mechanism can reproduce the results of the experiments to a very good accuracy. Therefore, this mechanism is utilised for further investigation.

Comparison of the simulated pressure curve and the experimental data for the three operating points during the different phases of combustion viz. ignition or early phase, centre of combustion and expansion phase, show very good agreement. As a result of the advanced ignition model in the form of flame kernel radius, an ignition progress parameter is presented. This parameter shows the effects of the conditions near the spark region on the flame progress. For the simulated operating points, changes in the flame kernel radius against the relevant changes in air-fuel ratio and pressure are

observed. In this way, it can be stated that, the advanced spark ignition model is able to reproduce ignition events for this type of engine with good accuracy.

Acknowledgement

Authors would like to thank EU for the funding to the GasOn Project (Project No 652816) in Horizon 2020 program, under which the presented work is carried out.

References

[1] G. Tallu, L. M. Beck, M. Prouvier, A. Winkler, M. Frambourg, and E. Shapiro. 3D CFD modelling and simulation of spark ignition inclusive turbulence effects and detailed chemical kinetics. *Ignition Systems for Gasoline Engines : 3rd International Conference, Berlin*, Addon:9–25, 2016.

[2] R. Maly and M. Vogel. Initiation and propagation of flame fronts in lean CH4-Air mixtures by the three modes of the ignition spark. *Symposium (International) on Combustion*, 17:821–831, 1979.

[3] R. Herweg and R. Maly. A fundamental model for flame kernel formation in S.I. engines. *SAE Technical Paper 922243*, 1992.

[4] Ansys Inc. *CHEMKIN MFC - Reaction Design*. Ansys Inc., San Diego, 2015.

[5] G. Smith, D. Golden, M. Frenklach, N. Moriarty, B. Eiteneer, M. Goldenberg, C. Bowman, R. Hanson, S. Song, Jr. W. Gardiner, V. Lissianski, and Z. Qin. GRI-MECH 3.0, 2014.

[6] L. Seidel, C. Netzer, M. Hilbig, K. Hoyermann, T. Zeuch, F. Mauss, P. Oßwald, K. Kohse-Höinghaus, and U. Stuckmeier. LOGEfuel Natural Gas Mechanism LOGE AB (Sweden), 2016.

[7] J. Huang, P. G. Hill, W. K. Bushe, and S. R. Munshi. Shock-tube study of methane ignition under engine-relevant conditions: Experiments and modeling. *Combustion and Flame*, 136(1):25–42, 2004.

[8] Y. Zhang, Z. Huang, L. Wei, J. Zhang, and C. Law. Experimental and modeling study on ignition delays of lean mixtures of methane, hydrogen, oxygen, and argon at elevated pressures. *Combustion and Flame*, 159(3):918–931, 2012.

[9] M. Elia, M. Ulinski, and M. Metghalchi. Laminar burning velocity of methane-air-diluent mixtures. *Journal of Engineering for Gas Turbines and Power*, 123(1):190–196, 2000.

[10] H. J. Neußer, J. Kahrstedt, H. Jelden, H. J. Engler, R. Dorenkamp, S. Jauns-Seyfried, and A. Krause. Volkswagen's new modular TDI generation. *33rd International Vienna Motor Symposium*, 2012.

[11] Heinzmann Gruppe. Gasmotorenmanagement : Produktkatalog. Technical report, Heinzmann GmbH & Co. KG, Münster, 2017.